Flexural behavior of hybrid fibre-reinforced geopolymer composites (FRGC)-jacketed RC beams

Guades, Ernesto J.; Stang, Henrik; Schmidt, Jacob W.; Fischer, Gregor

Published in:
Engineering Structures

DOI (link to publication from Publisher):
10.1016/j.engstruct.2021.112053

Publication date:
2021

Document Version
Publisher's PDF, also known as Version of record

Engineering Structures 235 (2021) 112053

Contents lists available at ScienceDirect

Engineering Structures

journal homepage: www.elsevier.com/locate/engstruct

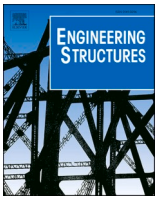

Flexural behavior of hybrid fibre-reinforced geopolymer composites (FRGC)-jacketed RC beams

Ernesto J. Guades [a,*], Henrik Stang [a], Jacob W. Schmidt [b], Gregor Fischer [a]

[a] Department of Civil Engineering, Technical University of Denmark, Lyngby, Denmark
[b] Danish Faculty of Engineering and Science, Section of Civil Engineering, Aalborg University, Aalborg, Denmark

ARTICLE INFO

Keywords:
Geopolymer
Fibre-reinforced geopolymer composites
Repair and strengthening
Jacketed RC beams

ABSTRACT

Fibre-reinforced geopolymer composites (FRGC) are drawing interest as potential repairing and strengthening materials for concrete elements due to their desirable properties. They are known to have good mechanical bond with the concrete substrate and steel reinforcement, good fire resistance, greater durability in corrosive environments, and lower creep and shrinkage characteristics. However, the main challenge in their practical application is the lack of design standards and the structural performance of FRGC-rehabilitated concrete elements has not been fully investigated. In this paper, the result obtained from an experimental study on the flexural behavior of reinforced concrete (RC) beams jacketed by hybrid FRGC is reported. Six repair and strengthening configurations were adopted in this study including jacketing at the bottom, two and three sides of the beam with at least 25 mm thick FRGC layer. Twelve FRGC-jacketed and two control beams were subjected to four-point bending test to determine their loading performance, cracking response, ductility and energy absorption capacity. In addition, an analytical model was developed to predict the ultimate moment capacity of the jacketed beams. The results showed that FRGC-jacketing technique increased the cracking, yielding and ultimate load of the initial RC beams by up to 167%, 62% and 62% respectively. Among the seven repair and strengthening patterns, the bottom and three-sides jacketing provided less ductile response, nevertheless, it offered a 32% increase on the energy absorption value of the initial RC beam. It also indicated that all jacketed RC beams displayed no sign of overlay delamination up to failure, confirming a bond excellence between the FRGC and concrete substrate. The model predicting the flexural moment capacity of the FRGC jacketed beams compared reasonably with the experimental results with error value of 4–7%.

1. Introduction

In the past decade, the fundamental properties of fibre-reinforced geopolymer composites (FRGC) had been widely investigated and draws interest as a promising material in the construction industry. One of the potential areas of application of this material is in the rehabilitation of structural concrete elements. FRGC are generally suitable for repairing and strengthening these elements since they are compatible with the concrete substrate [1,2],[3]. Accordingly, compatibility with the substrate is a key factor in the selection of suitable repairing and strengthening material [4,5]. Additional desirable properties for the use of geopolymer-based material in rehabilitating concrete structures include better fire resistance due to their ceramic-like properties [6] greater durability in severe environments, lower creep and shrinkage characteristics [7], and exhibited good bond with steel reinforcement [8],. Currently, FRGC has been field-applied for material repair in large-diameter sewer reinforced concrete (RC) pipes [9] RC culverts and sewerage manholes [10], and dam surface improvement [11], using spray-casting technique. In the context of structural repair and strengthening of concrete elements such as beams, to date no practical application has been documented. However, research studies on the use of FRGC in structural repair of RC beam shown positive result in reducing corrosion damage [12] enhancing cracking and bearing performance [12,13], matching the ductility with the counterpart RC beam [13] and is able to restore the flexural performance of the original beam [14,15].

In the present work, a more varied jacketing technique ranging from 1-side, 2-sides and 3-sides of the beam with different thickness layers (in the case of 1-side) was investigated since the mentioned studies on FRGC-strengthened RC beams did not simultaneously cover these three

* Corresponding author.
E-mail address: ergua@byg.dtu.dk (E.J. Guades).

https://doi.org/10.1016/j.engstruct.2021.112053
Received 18 April 2020; Received in revised form 5 February 2021; Accepted 9 February 2021
Available online 9 March 2021

techniques. Characterizing the flexural behavior of RC beams using other strengthening configurations provides wide-ranging understanding on the effectiveness of FRGC jacketing system. The present study used hybrid fibres as composite reinforcement in the repair and strengthening system as compared to mono-fibre reinforcement adopted in some literatures [12–14],[15]. Hybridization offers more attractive engineering properties including excellent toughening or energy absorption performance [16,17],[18] because the presence of one fibre enables the more efficient utilization of the potential properties of the other fibre [19],. Toughness of the composites as repair material is extremely important especially if the structure is under dynamic loading (i.e., seismic, impact or blast). Furthermore, as compared to the studies that are adopting blended geopolymer matrix [12], or cement-fly ash blend matrix [13–15] in jacketing RC beam, the present investigation attempted to use a 100% fly ash-based geopolymer matrix. The rationale of using a pure fly ash in the FRGC is to maximize its utilization since it is relatively cheap and abundantly available in landfill sites as compared to other geopolymer precursors [7,20]. Also, utilizing a 100% fly ash-based matrix in an FRGC also lead to reduced carbon dioxide emission than using Portland cement-fly ash blended composites.

This paper presents the experimental investigation on the flexural behavior of RC beams repaired and strengthened by hybrid FRGC using different jacketing configurations. Hybrid steel and Polyvinyl Alcohol (PVA) fibre reinforced geopolymer composite was used as repairing and strengthening materials. Twelve FRGC-jacketed and two RC control beams were subjected to four-point bending tests to determine their mechanical properties. The effect of the jacketing techniques was described in terms of the loading performance, cracking response, ductility and energy absorption capacity. In addition, an analytical model was developed to predict the ultimate moment capacity of the jacketed beams. It is expected that the output of this study can be used in the establishment of design standards and guidelines pertaining to the use of FRGC in repairing and strengthening structural concrete elements.

2. Experimental program

2.1. Material preparation and properties

The material and mix proportions of FRGC as jacketing material adopted in this study are listed in Table 1. The fly ash used is Class F (low calcium) and conformed to EN 450–1 [21], with the chemical composition shown in Table 2. Silica sand with particle diameter ranging from 0.06 to 2.00 mm and specific gravity of 2.64 was used as fine aggregate. Straight steel fibre and PVA fibre having a length of 11 mm and 18 mm, respectively (properties are shown in Table 3) were used in the study. A total fibre volume content of 2% (i.e. 1% steel fibre and 1% PVA fibre) was chosen based from the conducted trial mixture since at this level the mortar mixture remained workable. A combination of 12 M sodium hydroxide (NaOH) solution and sodium silicate (Na_2SiO_3) was used as alkaline activator (AA) with a ratio of Na_2SiO_3/ NaOH solution of 2.5. The adopted AA to fly ash (FA) ratio is 1 while the sand to (FA + AA) ratio is 3. In preparation for FRGC mixture, the alkaline activator was prepared 24 h before the actual mixing. Fly ash and sand was dry mixed in a pan mixer for 5 min and then alkaline activator was added and mixed for another 5 min. After 5 min wet-mixing, steel fibres were added gradually and mixed for another 3 min before the addition of PVA fibre. Mixing continued for another 5 min after the addition of PVA fibre resulting to a total FRGC mixing time of 18 min. To determine the mechanical properties of hardened FRGC (compressive and tensile strengths), the prepared FRGC wet mixture was poured in a desired mould and cured before the actual tests. The specimens were initially cured in a 50 °C temperature-controlled chamber with 98% relative humidity for 48 h, after which they are demoulded and stored in an ambient temperature room and tested after 28 days. The compressive properties of the used FRGC was characterized by testing of 5 cylindrical specimens having a size of 60 × 120 mm in a compressive testing machine. On the other hand, the tensile properties of FRGC were determined by testing 3 dumbbell-shaped specimen with a test cross section of 40 × 40 mm in a uniaxial testing machine. Compressive and tensile test specimens were all instrumented by extensometer to record their respective strain values. Figs. 1 and 2 shows the testing set-up and the samples of stress–strain curves from compressive and uniaxial tensile tests. The average compressive and tensile strength values, as well as the modulus of elasticity of the FRGC obtained from the test is 18.9 MPa, 3.5 MPa and 21 GPa, respectively. The result obtained from the tests indicates that the specimen subjected to tensile load underwent softening behavior after reaching its peak load capacity. Due to this behavior, multiple-crackings on the surface of the specimen was not observed in all of the tested specimens.

The concrete used in casting the RC beam was made from a mixture of ordinary Portland cement, sand (0.1–2.00 mm particle size) gravel (8–16 mm particle size) and water with mixture combination displayed in Table 1. During casting of initial RC beams, 5 companion cylindrical samples (100 × 200 mm) were prepared and tested for compressive strength. The test result showed that the mean compressive strength of concrete at 28 days is 21.5 MPa. For steel reinforcements, the average value of the yield strength and ultimate strength of the used 10 mm diameter main reinforcement were 442 MPa and 587 MPa, respectively, based on tensile tests of 3 specimens. On the other hand, the result on the tensile test for 6 mm diameter shear reinforcement used in the RC beam showed that the average value of the yield strength and ultimate strength were 487 MPa and 582 MPa, respectively.

2.2. Beam preparation and FRGC jacketing method

Fourteen RC beams (2 replicates for each jacketing configurations and 2 replicates as control specimens) were investigated in this study. All beams have a length of 1,100 mm with a nominal cross section of 100 × 150, 150 × 150 mm and 150 × 175, depending on the applied jacketing configurations. Table 4 displays the jacketing configurations and the test beam dimensions used in this investigation. In this study, jacketed beams were clustered into 2 groups, namely repaired beams and strengthened beams whose description is basically related to the cross section of the control specimen. Repaired beams correspond to test beams having identical cross section with the control specimen resulting to the addition of FRGC overlay. On the other hand, strengthened beams resemble to test beams with bigger cross section relative to control specimen as a consequence of adding FRGC layers to the latter. The thickness of the FRGC overlays for strengthened beams adopted in this study is in the range of 25–66 mm. Proper labels were assigned to beam specimens, where R stands for repaired, S for strengthened, t for thickness of FRGC overlay, 1 J for FRGC overlay placed on the bottom of the beam, 2 J for FRGC overlay placed on the 2 sides of the beam and 3 J for FRGC overlay placed on the bottom and 2 sides of the beam. In the case

Table 1
Mix proportion of FRGC and concrete.

Material	Unit Content [kg/cu^3]								
	Fly ash	Cement	[a]Alkaline Activator	Sand	Gravel	Water	Superplasticizer	Steel fibre	PVA fibre
FRGC	486	–	486	1,458	–	–	–	78	13
Concrete	–	300	–	930	960	180	3	–	–

[a] Breakdown of Alkaline Activator: Na_2SiO_3 = 347 kg, NaOH Pellets = 54 kg, dionized water = 85 kg

Table 2
Chemical composition and property of fly ash [21],

Chemical Composition	SiO_2	Al_2O_3	Fe_2O_3	CaO	Na_2O	SO_3	Cl	LOI	Specific gravity
Value [% of Mass]	56.4	21.6	5.4	3.9	2.9	0.6	≤0.05	2.1	2.30

Table 3
Properties of fibre reinforcement.

Fiber type	Nominal length, L (mm)	Nominal diameter, d (μm)	Aspect ratio, L/d	Density (kg/m^2)	Youngs modulus (GPa)	Tensile strength (MPa)
Steel fibre	11	390	28	7.85	200	1,100
PVA fibre	18	200	9	1.3	30	975

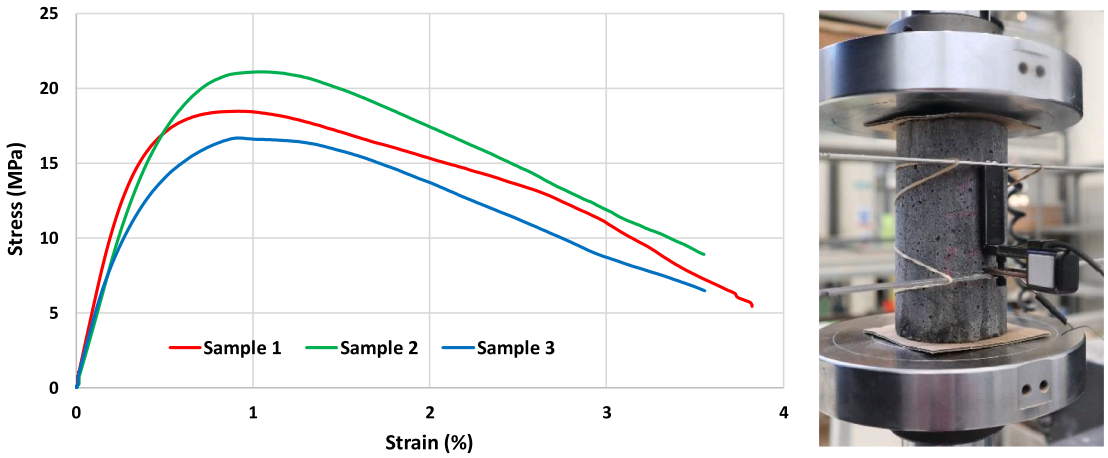

Fig. 1. Compressive stress–strain curve and testing set-up for FRGC specimen.

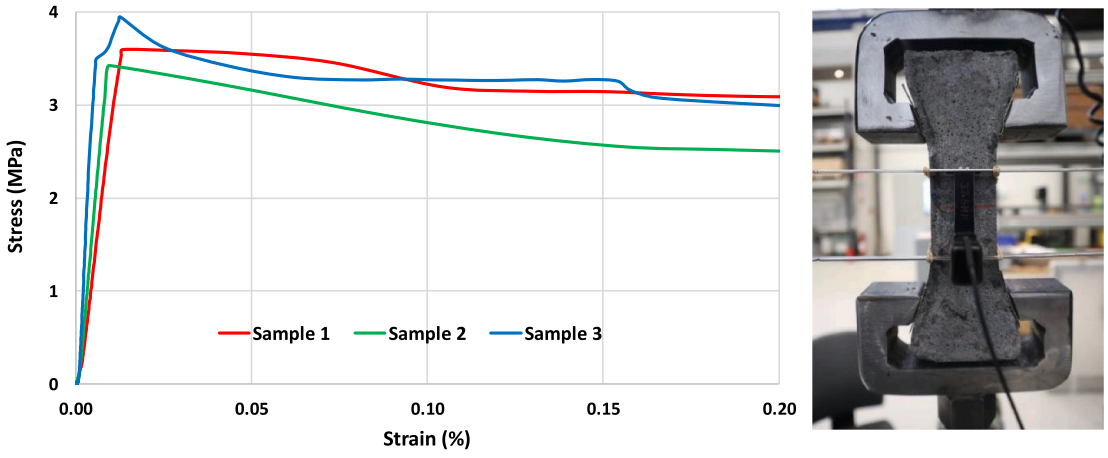

Fig. 2. Tensile stress–strain curve and testing set-up for FRGC specimen.

of RS-t66, both R and S are indicated in the label since this beam can be considered to be both repaired and strengthened specimen. Beam specimens were provided with a main reinforcement of two 10 mm diameter steel bars at the tensile zone and stirrups of 8 mm diameter with 90 mm spacing, as shown in Fig. 3. The initial beams were prepared according to the concrete mixture in Table 1 and casted to the desired cross section. After demoulding of the initial beam specimens, they were wrapped in plastic sheets and matured for 60 days (Fig. 4a).

Sixty days after the initial beams was casted, the surfaces of the beam were roughened using a needle scaler (Fig. 4b) and cleaned using high pressure washer water jet gun. The beams were left to dry with the use of air pressure spray drying machine, after which they were placed in a mould (Fig. 4c) in reference to the desired jacketing configurations shown in Table 4. FRGC was prepared using the mixture in Table 1 (Fig. 4d), after which repair and strengthening procedures were performed by adding new FRGC layers on the beams (Figured 4e). One of the challenges faced by the study is on the curing process of FRGC or FRGC-strengthened RC beams since it was conducted during near-winter time. For the FRGC material where a 100% fly ash was used, it needs higher temperature (at least at ambient condition or at higher temperature up to 60 °C) to aid in the geopolymerisation process and curing. As a result, repaired and strengthened beams were placed and initially cured in a 50 °C temperature-controlled chamber with 98% relative humidity for 48 h, after they were demoulded and stored until testing

Table 4
Jacketing configurations and nominal test beam dimensions.

Repair and Strengthening Configuration	Specimen ID	Overall depth, D (mm)	Overall width, B (mm)	FRGC overlay thickness, t (mm)	Number of test beams
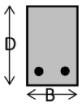	RC_Control	150	100	–	2
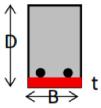	R-t25	150	100	25	2
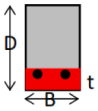	R-t41	150	100	41	2
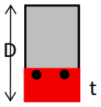	RS-t66	175	100	66	2
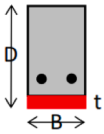	S-1 J	175	100	25	2
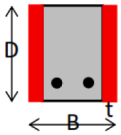	S-2 J	150	150	25	2
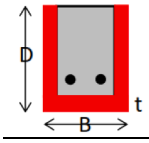	S-3 J	175	150	25	2

day. For the practical application of the proposed strengthening technique in some cold regions, it is recommended that this method can be undertaken during the summer time where temperature is generally higher. In the case of tropical areas where climate is characterised by warm to hot, the in-situ application of the proposed strengthening technique maybe applied year-round. Fig. 4 shows the repair and strengthening procedure and the beam specimens ready for testing.

2.3. Test set-up and procedure

Fig. 5 presents the typical test set-up and instrumentation details of the study. All beams were loaded in a four-point bending using a 100kN-capacity testing machine under displacement control rate of 2 mm/min. The effective test length of all specimens is 950 mm and was loaded symmetrically at two points 200 mm apart about its centerline. For this set-up, the size of the test beams (at least the control specimen) is adequate for pure flexural behavior since it fulfilled the condition of shear span to depth ratio ≥ 2. A 20 mm length strain gauge was glued on the bottom surface of each specimen at mid-span while one linear variable displacement transducers (LVDT) was placed at the bottom mid-span to record the specimen deflection. An automatic data acquisition system was used to record the loading, deflections and strain values. Visual inspection was performed on the specimens while the test progresses to document initiation and propagation of cracks until the beam reached failure. In all of the bending tests, the complete beam failure (i.e. rupture of reinforcement steel) were not obtained and tests were stopped once the concrete in the compression zone started crushing to protect the mounted LVDT from potential damage.

3. Experimental results and discussion

3.1. Load-deflection relationship

The load–deflection relationship of RC control beam, as well as beams subjected to different repair and strengthening patterns are shown in Figs. 6–7. Note that the values plotted in the figures were taken from one of the two test beams of each pattern. The control specimen exhibited the expected flexural response of a ductile (tension-controlled) beam whereby the steel reinforcement yielded prior to crushing of the concrete in the compression zone. The load–deflection response of the control beam can be approximated into three stages, whereby the first stage represents the behavior during un-cracked condition which depends primarily on the gross moment of inertia (or cracking resistance of the concrete in tension zone). This happened at a load level of approximately 7.6 kN. The second stage describes the post-cracking condition up to yielding of steel reinforcement at 40.6 kN, which in turn represents

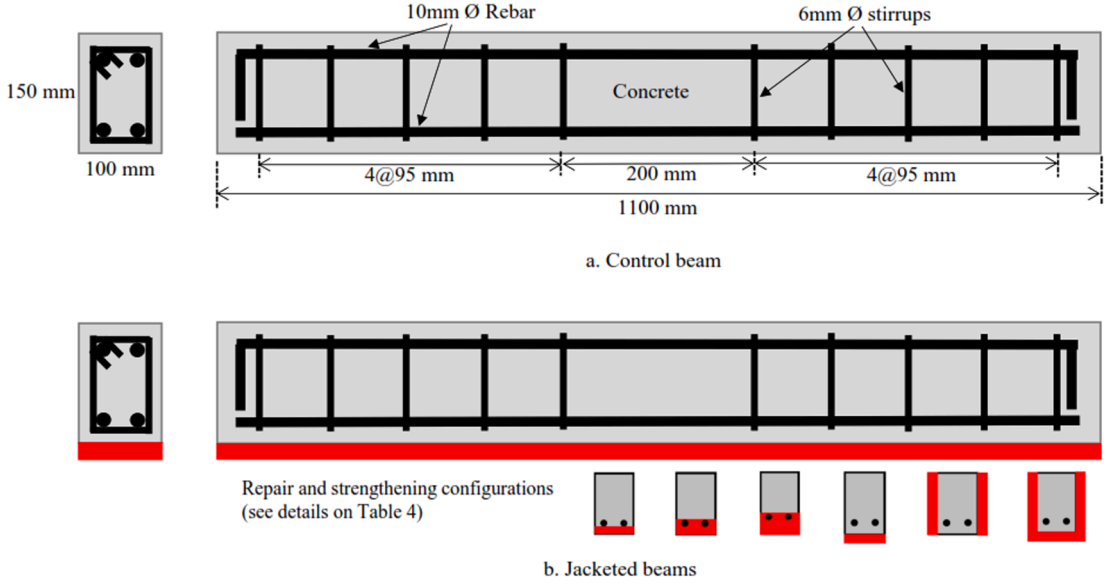

Fig. 3. Reinforcement details and geometry of the tested beams.

a. Casted initial RC beam b. Roughening of RC beam c. Placement of RC beam

d. Preparation of FRGC e. Pouring of FRGC f. Jacketed RC beam

Fig. 4. Repair and strengthening procedure using FRGC.

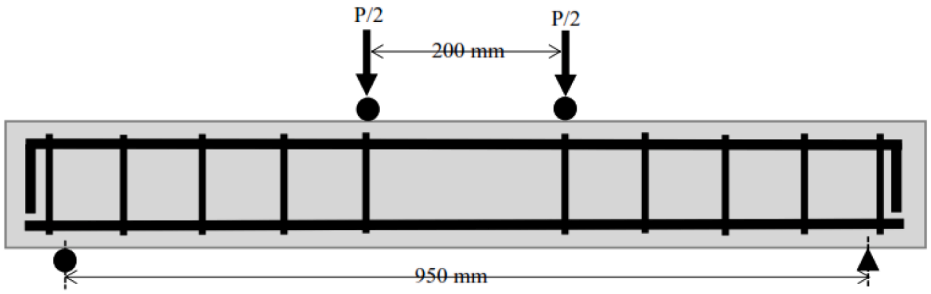

a. Schematic diagram

b. Actual test

Fig. 5. Experimental set-up of 4-point loading test.

the cracked beam that resulted in decreased moment of inertia. These two stages constitute the elastic region as indicated by the change of slope in the curve. The last stage, representing the steel yielding up to the ultimate condition before reaching the final beam failure at 42.3 kN loading, describes the inelastic region.

The trend of the load–deflection curves in Fig. 6 for repaired beams (i.e., R-t25, R-t41 and RS-t66) is identical to that of the control beams. Based on visual observation of the specimen and the progressive load–deflection curve displayed on the monitor during the actual test, generally the failure of all repaired beams was by rupture of the FRGC overlaid layer within the mid-span, after yielding of the bottom steel reinforcement and before crushing of concrete in compression. Just like

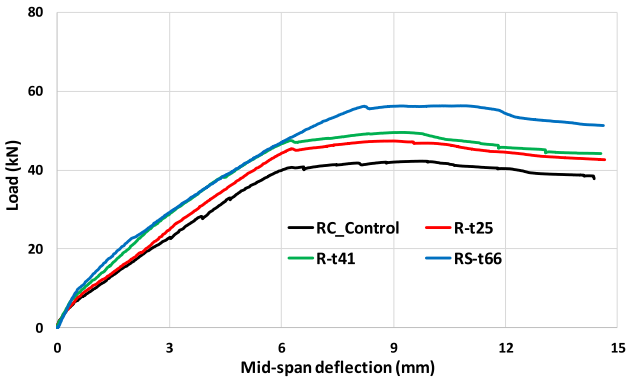

Fig. 6. Load-deflection relationship of repaired RC beams.

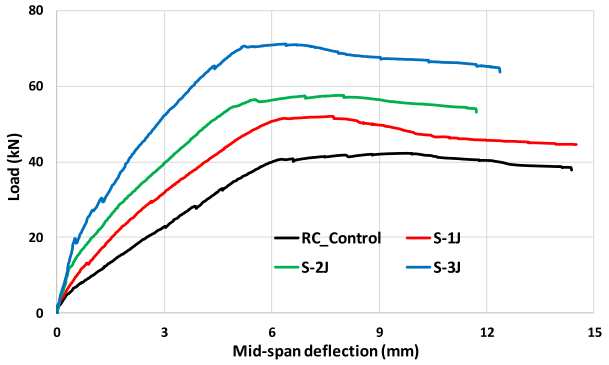

Fig. 7. Load-deflection relationship of strengthened RC beams.

the failure mode of the control specimen, repaired beams at ultimate loading conditions failed by crushing of concrete at the compression zone and no delamination between the FRGC and concrete substrate was observed. Three stages starting from un-cracked, cracking to yielding of steel, and yielding of steel to crushing of concrete in the compressive zone with different lengths of elastic and inelastic regions are noticeable. Beam R-t25 exhibited identical behavior as RC control except that load slightly increased with more improved stiffness up to initial cracking and yielding of reinforcement at 7.4 kN and 45.4 kN, respectively. The linearity of the first cracking region indicates that at this stage the constituent elements of R-t25 (i.e., 25 mm thick FRGC and initial RC beam) provided composite action to sustain a load up to 7.4 kN. After yielding, the load increase narrowed down indicating that FRGC released its tensile contribution and is undergoing softening behavior (evidenced by Fig. 2). Compared to RC_control, the length of the first part of the elastic region for R-t25 is relatively long, credited primarily to the improved cracking resistance offered by FRGC overlay. The first elastic region is where the FRGC and concrete in the tension zone act monolithically as composites in resisting applied load before cracking. Unlike RC_Control where the first cracking is usually dependent on the cracking resistance of the concrete, the first cracking performance of R-t25 specimen is contributed by both FRGC overlay and concrete in tension zone. After cracking, the curve entered the second part of the elastic region with relatively smaller slope than the first elastic zone. The curve approaches the inelastic region when the bottom steel yielded at a load level of 45.2 kN and followed a slight upward slope before reaching the peak load. At this stage, crushing of concrete on the compression zone commenced and continuously dropping the load after sustaining additional deflection until the stoppage of the test.

Similar load–deflection responses were observed for R-t41 and RS-t66 as shown in Fig. 6. Cracking of R-t41 happened at a load level of 8.3 kN while yielding of bottom bars and crushing of concrete in compression occurred at 47.3 kN and 49.6 kN, respectively. No clear difference between the stiffness values in the first elastic region can be established between the repaired (i.e., R-t25 and R-t41) and control beams, however it is apparent that the length of this region of the former is longer than the later. Evidently, the FRGC material prolonged the first elastic region of the repaired beam by delaying the occurrence of crack. FRGC is known to have better cracking resistance compared to plain concrete due to their higher tensile strength. Comparing the lengths of the second elastic region (i.e., post cracking to steel yielding), RS-t66 and R-t41 exhibited longer lengths than control specimen and R-t25. This implies that a much higher load and larger deflection are required for the bottom reinforcement of RS-t66 and R-t41 to yield. Steel reinforcement has a better bond performance with FRGC (in the case of RS-t66 and R-t41) compared when it is combined with plain concrete (in the case of control specimen and R-t25). While fibre reinforcement improves the rebar-to-concrete bond by providing additional confinement effect [22], and reduced the tensile stress in the rebar [23] fly ash-based geopolymeric matrix exhibited better bonding than its cement-based counterpart [8],. This synergistic composite property leads to strain localization in the FRGC-to-rebar interface with reduction of the portion of the strain in rebar, thus increased the yielding load and deflection values of the RS-t66 and R-t41 specimens.

The load–deflection relationship of the strengthened beams (i.e., S-1 J, S2J and S-3 J) likewise follows a trilinear curve as shown in Fig. 7. One can observe that generally the stiffness in the first elastic region of the strengthened beams is higher than the control specimen. It is also apparent that the length of the first elastic region for strengthened beams is longer than the control specimen. S-1 J exhibited slight increase in both slope and length in this region relative to RC_Control with crushing of concrete as the actual failure at peak loading condition. This enhancement is primarily attributed by the addition of FRGC section that consequently increased the un-cracked gross moment of inertia. At the first elastic zone (i.e., load level of 12.9 kN), S-1 J remained intact and act monolithically, which is the same response exhibited by Rt-B66. One major difference that can be established between these two specimens is that the length of the first cracking region for S-1 J is shorter than RS-t66. Although these specimens have equal nominal cross sectional areas, the amount of FRGC incorporated for S-1 J is relatively smaller than RS-t66, thus the contribution in increasing the load–deflection values is minimal. On the other hand, the length and slope of S-2 J in the first cracking region have an intermediate values between S-1 J and S-3 J. Relative to the control specimen, the enhancement was provided by the stiffening effect of the added FRGC on the two sides of the RC beam. Just like S-1 J, S-2 J responded monolithically and no delamination between FRGC and the concrete substrate was observed in the first cracking region. The typical failure at ultimate condition for S-2 J was either crushing of concrete or FRGC at the compression zone. S-3 J exhibited the highest increase in slope and length in this zone due to the maximum equivalent addition of FRGC, hence highest relative un-cracked moment of inertia. An utmost value of slope is also noticeable for S-3 J than the other strengthened beams with more significantly relative to the RC_Control. This is certainly demonstrating the effectiveness of jacketing the three sides of the beam using FRGC in not reducing the load rapidly after the occurrence of first cracking. In contrast, the transition in the inelastic region for S-3 J is generally shorter with a sudden softening mode, indicating a less ductile failure compared to S-1 J, S-2 J and conventional RC beam. This shows that addition of tension reinforcement by means of jacketing at the three sides using FRG can essentially transform the behavior of the originally under-reinforced section to that of an over-reinforced one. Increasing the amount of effective tension FRGC lowers the location of the neutral axis that triggers either FRGC and concrete approached their compressive crushing strain. The crushing of these two component materials prior to any significant post-yielding of the steel will lead to the undesirable brittle mode of failure. Nevertheless, S-3 J exhibited a monolithic response with no observed debonding between FRGC and concrete substrate during the entire flexural test. Similar with S-2 J, the failure

mode of S-3 J at ultimate loading condition was either crushing of concrete or FRGC at the compression region.

3.2. Loading capacity of tested beams at different stages

Table 5 summarizes the load values (average of 2 replicates) of beam specimens at different loading stages and its normalized values are graphically presented in Figs. 8–9 for ease of comparison. Results shown in Table 5 indicated that the first cracking load of repaired RC beams is in the range of 8–10 kN, depending on the thickness of FRGC material and its interface location with the concrete substrate. The first cracking in the repaired beam may occurred theoretically at the FRGC section and/or the concrete in tension, although it has been observed in the tests that cracking usually started at the FRGC layer (previously highlighted). As illustrated in Fig. 8, cracking for R-t25 initiated at a load level of 8.06 kN, a value that is 28% higher than the control specimen. The increase is attributed from a relatively high tensile strength of FRGC. At same cross-sectional area, a thicker 41 mm FRGC added on the bottom of the control beam (i.e., beam R-t41) resulted in an 8.27 kN first cracking load capacity. This repair configuration magnified the cracking performance of the beam by 31% relative to the control and slightly higher by 3% on R-t25. Increasing the thickness of the repair material to monolithic 66 mm (beam RS-t66) lead to a first cracking load of 9.96 kN that somehow increased the capacity by 60% compared to the controlled specimen. Unlike R-t25 and R-t41, this time the initial cracking resistance of RS-t66 is attributed by the dual contribution of the excellent tensile properties of FRGC and the increased moment of inertia effect with its addition on the beam soffit. The increase of cracking load is also evident by observing the cracking strain value whereby the value of repaired beams is approximately 3–4 times that of RC_Control.

On the other hand, the yielding load of the repaired beams is in the interval of 45–56 kN, R-t25 expectedly showing the least exhibition of yielding load having a marginal 8% increase relative to the RC_Control. Comparing the load interval difference from cracking to yielding point of R-t25 and control beam (i.e., 36.9 and 35.3 kN, respectively) provided a value of 5% which can be considered as a negligible difference. Ergo this indicates that the increase of yielding load of the former is only primarily due to the initial cracking resistance provided by FRGC and the replacement of ordinary concrete with same cross section of FRGC will not significantly alter the yielding load response of the bottom reinforcement bar. Thickening the FRGC section to 41 mm in a repaired beam (i.e., R-t41) outperformed the yielding load response of the control beam and R-t25 by 14% and 6%, respectively. Unlike R-t25, the load increment from cracking to yielding point of R-t41 is 17% higher than the control specimen. Noted that in this particular repairing method the originally normal concrete-rebar bond has been replaced by FRGC-rebar interface as a result of repair material thickening. Certainly the excellent FRGC-rebar bonding performance modified the favorable yielding load response of the bottom steel reinforcement. The reason is because FRGC reduced the applied tensile strain in the rebar through strain localization at the interface resulting to a much higher load value for the rebar to yield, as discussed earlier. This finding is noteworthy in the sense that not only for this specific repair configuration the bottom rebar can be protected from further corrosion, if there is, but will also help in enhancing its yielding capacity resulting to a much better loading performance. As expected, RS-t66 exhibited the greatest yielding load at a load level of around 55.9 kN, a value that is 35% higher than the control specimen whose enhancement is primarily due to a much larger FRGC cross section and excellent FRGC-rebar bonding chemistry. Meanwhile, the ultimate loading capacity of the repaired beams is slightly higher than its corresponding yielding load and is in the vicinity of 47–56 kN. Fig. 8 indicates that the ultimate loading capacity of beam R-t25 is 10% higher than the control specimen while R-t41 exhibited a 17% enhancement. This result demonstrates that these repair techniques are effective in restoring or even improved the original ultimate loading capacity of the monolithic beam depending on the thickness of the FRGC repairing material. R-t66 also showed a better ultimate load

Table 5
Load values of tested beams at different stages.

Specimen ID	First cracking		Yielding load (kN)	Ultimate load (kN)
	Load (kN)	Strain (%)		
RC_Control	6.29	0.0019	41.52	42.34
R-t25	8.06	0.0057	44.99	46.62
R-t41	8.27	0.0071	47.33	49.55
RS-t66	9.96	0.0082	55.89	56.31
S-1 J	12.20	0.0059	51.30	51.30
S-2 J	12.62	0.0020	56.34	57.59
S-3 J	16.77	0.0074	67.47	68.63

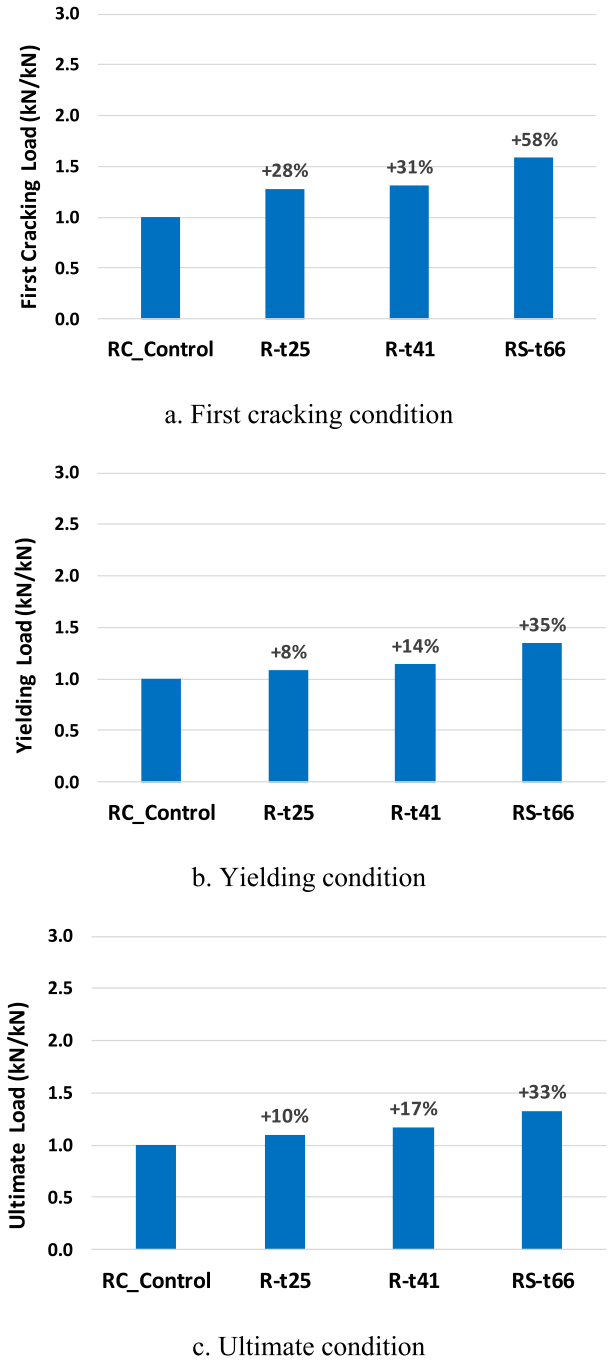

Fig. 8. Normalized load values at different stages for repaired beams.

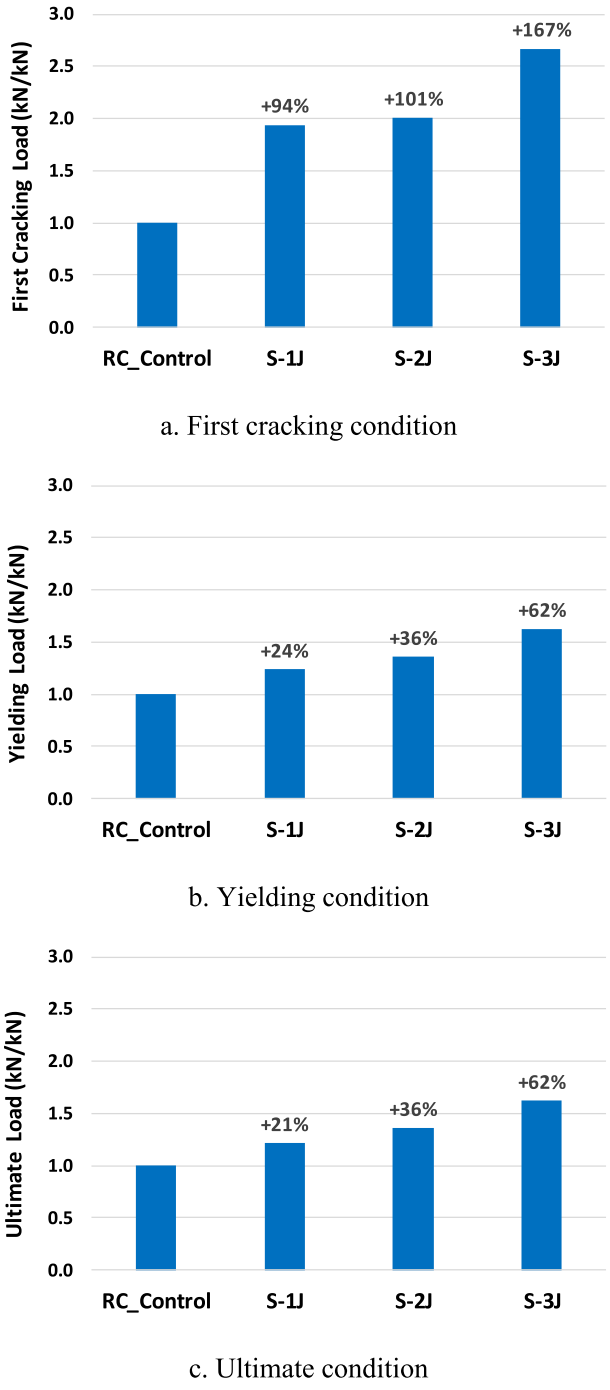

Fig. 9. Normalized load values at different stages for strengthened beams.

performance by getting a value of 33% higher than the control specimen. In general, the enhancement of the ultimate load capactiy of the repaired beam is attributed by the superior cracking performance of the FRGC and its excellent adhesion properties with the tensile reinforcement bar.

The effects of the three jacketing techniques applied at different sides of the beam on the loading performance of the strengthened specimens are displayed in Fig. 9. As expected, the experimental results shown in Fig. 9 indicate an increase of varying degrees in the load performance for all of the strengthened beams relative to the control beam as a result of an enhanced stiffening action provided by FRGC strengthening layer. These techniques were able to demonstrate an initial cracking load capacity at a load level between 12 and 17 kN, depending on the number of jacketed sides. In the case of jacketing at the bottom side, this technique was able to increase the load to initially crack the beam by 94% higher than the control beam, whereas jacketing at the two sides of the beam yielded 101% enhancement. While the improvement on the cracking load of S-1 J was attributed due to the increased un-cracked moment of inertia solely in the tension zone, the un-cracked moment of inertia of beam S-2 J generally is obtained from both compression and tension regions. Consequently, the first cracking load of S-2 J may exhibit higher value than S-1 J, just like the case in the present study whereby the result of the former showed marginally higher value of 7% than the latter. Similarly, beam strengthened by 3-sides jacketing technique has improved first cracking performance showing the highest increase of 167% compared to the control beam. The highest increase in this aspect for S-3 J is anticipated as a result of adding FRGC on the three sides of the beam causing a remarkable growth of the un-cracked moment of inertia in both compression and tension zones. It can be seen from Table 5 that strengthened beams generally cracked at relatively higher strains than that of RC_Control indicating that apparently the former was subjected by loads higher than the latter.

Beams strengthened using the three jacketing techniques demonstrated yielding load ranging from 51 to 69 kN, as can be seen in Table 5 and Fig. 9. Compared to the RC_Control, jacketing the beam only at the bottom increased the yielding load capacity by 24%. Once cracking initiated on either FRGC or concrete at the tensile zone and later extend to the bottom reinforcement bar, applied load to the beam S-1 J will only now be resisted by the yielding capacity of the rebar and the concrete section at the compression zone, that eventually will behave just like an ordinary RC beam. Changing the jacketing configuration from the bottom to the two sides of the specimen exhibited 36% increase of load to yield the strengthened beam. Unlike the post-cracking-to-yielding response of S-1 J were the yielding load is partially contributed by the concrete section at the compression zone, the yielding load of S-2 J is provided by both FRGC and concrete sections. This phenomenon can be supported by the result of the present study wherein S-2 J exhibited 12% higher yielding load than S-1 J. Referring from Table 5, the initial cracking load increment for S-1 J and S-2 J can be calculated as equal to 7% while their post-cracking-to-yielding load deviation is 12%. These values indicate that the contribution of the initial cracking load response to improve the yielding performance from 1-sided (bottom) to 2-sided jacketing technique seems to be less significant than the post-cracking-to-yielding load response. Meanwhile, applying a 3-side jacketing approach to strengthen the beam showed a relatively high yielding load increase of 62% than its un-strengthened counterpart. Regarding the ultimate load capacity of the strengthened beams, the trend is similar to that in the first cracking and yielding conditions in which S-1 J and S-3 J demonstrated the least and largest value, respectively. Strengthening RC beam using bottom jacket increased the ultimate loading value by 21% while jacketing the three sides resulted to 62% load rejuvenation. The ultimate loading capacity of the beam jacketed at the two sides remained intermediate relative to beams S-1 J and S-3 J, obtaining 36% higher value than the control specimen. The increase may be credited to the fact that the rigidity of the jacket, regardless the type of configuration used, makes it the significant part in carrying the load compared with the un-strengthened beam.

Comparing the effects of the different repairing techniques to enhance the loading capacities of the beams, it seems that the load at the first cracking stage has been the most resonated value than at the yielding and ultimate conditions as demonstrated in Fig. 8. The first cracking load increase is around 28–58% while only 8–35% and 10–33% at yielding and ultimate conditions, respectively, can be generated. This is also true for strengthened beams jacketed at the bottom, two and three sides in which the increase of the first cracking load are considerably higher than the increase of their corresponding yielding and ultimate capacities (Fig. 9). This definitely indicates the effectiveness of FRGC to bridge the crack and delay the occurrence and propagation as a result of its inherent high crack resistance. In the rehabilitation of deteriorated

RC elements with corroded steel reinforcement, the inherent relatively higher cracking load of the FRGC is an advantage as it can prevent the occurrence of re-deterioration.

3.3. Ductility performance of the tested beams

Ductility in RC beam maybe defined as its ability to sustain deformation beyond the elastic limit while maintaining a reasonable load carrying capacity until total failure [24] and is one of the design parameters that needs to be identified to ensure desirable failure of the structural element. The addition of FRGC layer may not only provide positive impact on the RC beam in terms of increased the strength and stiffness but may also contribute in reducing its ductility. In the present study, ductility was described using an index in terms of deflection and quantitatively defined as the ratio between the deflection at peak load δ_{max} and the deflection at yielding load δ_y. Table 6 summarizes the ductility indices of the test specimens and the normalized values with respect to RC_Control are plotted in Figs. 10–11 for comparison. Fig. 10 illustrates that the ductility was increased when plain concrete was replaced by FRGC to restore its original cross section depending on the thickness repairing material. R-t25 demonstrated marginal ductility increase of 3% relative to the control beam. This indicates that a 25 mm FRGC replacement is not enough to significantly lower the neutral axis that leads to subsequent reaching of the compressive concrete crushing values soon after yielding of the beam tensile reinforcement. Assuming that total ruptures of the tensile FRGC happened before yielding of concrete, then the deflection response of R-t25 resembles that of the control beam indicating their respective ductility indices are getting comparable values, as evidenced by Fig. 10. Repairing the beam by a thicker 41 mm of the FRGC material resulted in a 1.46 displacement ductility that brought an increase of 5% and 8% relative to R-t25 and control specimen, respectively. Compared to R-t25, increasing the thickness from 25 mm to 41 mm tends to level up the effective tension FRGC that eventually lift the location of the neutral axis closer to the concrete extreme edge compression zone. The upward movement of the neutral axis has led to the reduction of the amount of strain introduced to the concrete in compression, thus allowing the beam to deflect more before attaining its crushing strain. It is suspected that the enhanced ductility was also provided due to the excellent FRGC-rebar bonding, that allows the yielded rebar to fully develop the plastic deformation before crushing of concrete in the compression zone. Among repaired specimens, RS-B66 showed the lowest ductility index corresponding to 7% and 12% lesser than R-t25 and R-t41, respectively. The addition of extra 25 mm thick FRGC in reference to R-t41 starts RS-t66 to resemble more that of an over-reinforced concrete beam. In general, beams repaired using these three patterns showed promising results of not only a providing a noticeable increase in ultimate capacity, but also without an appreciable compromise on the ductility of the structure.

Fig. 11 shows that the jacketing technique on the bottom, two and three sides of the beam provided conflicting effects on the ductility behavior of the strengthened specimens. In the case of S-1 J, jacketing method provided a less favorable outcome that marginally decreased the ductility index by at least 7%. Putting equivalent thickness of 25 mm FRGC on the two sides of the beam (S-2 J) increased the ductility of the RC beam by 3%. Beam S-2 J exhibited higher ductility index value than

Table 6
Ductility indices of the tested beams.

Specimen ID	δ_y (mm)	δ_{max} (mm)	Ductility index, δ_{max}/δ_y
RC_Control	6.55	8.88	1.36
R-t25	6.12	8.56	1.40
R-t41	6.31	9.23	1.46
RS-t66	8.29	10.81	1.30
S-1 J	6.23	8.88	1.26
S-2 J	5.61	7.86	1.40
S-3 J	5.36	6.47	1.21

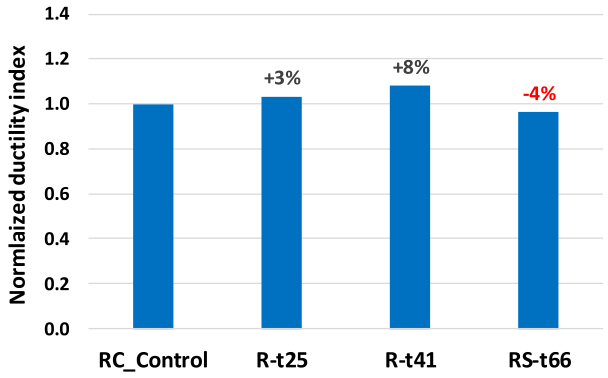

Fig. 10. Comparative curve of ductility performance for repaired beams.

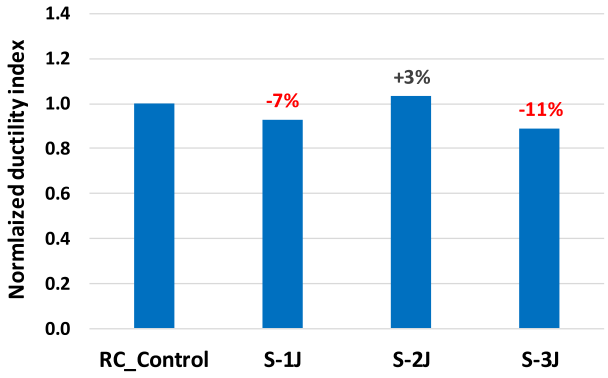

Fig. 11. Comparative curve of ductility performance for strengthened beams.

S-1 J since theoretically placing 25 mm thick FRGC on the two sides of the beam provided smaller effect in lowering the neutral axis than putting it on bottom. As a result, S-2 J required longer deflection after post-yielding of steel to reach the crushing strain of concrete in compression. Moreover, putting fibre reinforcement by virtue of FRGC on the upper part of the beam avoid a sudden and brittle concrete crushing owing to their ability of enhancing concrete toughness in compression [25] thus increased ductility. Beam S-3 J demonstrated an opposing ductility performance as the index value is reduced by 11% compared to that of RC_Control. While the provision of jacketing the three sides of the beam provided the highest increase of load capacity, this technique offered a ductility performance of 4% and 16% lower than S-1 J and S-2 J, respectively. Compared to S-2 J, the less ductile performance of S-3 J may be attributed to the addition of equivalent tensile FRGC on the bottom that significantly resonate the crushing strain at the compression region. The result obtained in the present study seems to be consistent with that of the result on cement-based fibre-reinforced strengthened RC beams whereby three-side jacket provided less ductile performance than bottom and two-side jacketing techniques [26],.

3.4. Energy absorption capacity of the tested beams

The energy absorption capacity of composites as repair material is extremely important especially if the structure is under dynamic loadings (e.g., seismic, impact or blast) and FRGC are favorably suitable in these applications. The ability to absorb energy corresponds to the toughness of the material and is associated with the deflection hardening behavior of the composites [27],. In fibre-reinforced concrete, theoretically macro-fibres (i.e., steel) increase the composite toughness by bridging macro-cracking while micro-fibres (PVA) enhanced the response to micro-cracking prior to the formation of macro-cracks [28],. If synergized, it is expected that micro-fibres enhance the pull-out

capacity of the macro-fibres resulting in composites with high strength and toughness [29],. In this study, the energy absorption capacity of the beams was obtained by calculating the area under the load–deflection curve extending up to the ultimate loading condition. Fig. 12 mirrors the superior performance of FRGC-repaired beam in terms of the energy absorption capacity over the unrepaired beam at varying degrees. For instance, R-t25 demonstrated that it can absorbed energy up to 310 kN-mm, a value equivalent to 21% more than the control specimen can do. Likewise, thickening the FRGC repair material to 41 mm (R-t41) yielded a 25% increase in the energy absorption capacity. RS-t66 showed the most magnified absorption capacity at an energy level of 429 kN-mm indicating a 68% increase relative to the control beam. This result indicated that the ability of the repaired beams to absorbed energy increases with the amount of the replacing material that was attributed mainly due to the excellent toughening effect of the FRGC, as evidenced by Fig. 12.

Similarly, strengthened beams using FRGC jacket at the bottom, two and three sides exhibited higher absorption capacity than unstrengthened counterpart, as demonstrated in Fig. 13. Jacketing at the bottom (S-1 J) led to an absorption capacity value of the beam to 270 kN-mm, corresponding to 6% more energy it can absorb if the beam is not jacketed. On the other hand, S-2 J and S-3 J offered almost identical absorption performance exhibiting an absorbed energy of 331 kN-mm and 337 kN-mm, respectively. Although S-3 J demonstrated a relatively high ultimate load capacity than S-2 J (30% in this case), its deflection to reach at the ultimate condition is shorter than the latter that resulted to a marginal difference of only 2% on their energy absorption capacity. Nevertheless, jacketing on the two and three sides of the beam can be considered effective toughening technique since they can absorb 30% and 32%, respectively, more energy than without putting jacket at all. Unlike in the case of repaired beams in which the toughness interval is solely dependent on the amount of equivalent tensile FRGC, it seems that for strengthened beams the jacketing patterns (i.e., bottom, two and three sides) also matters as evidenced by a tapered interval value of 2% between S-2 J and S-3 J.

3.5. Cracking behavior and failure mode

The cracking characteristics and patterns at failure of control, repaired and strengthened beams are shown in Table 7 and Figs. 14–16. Control beam demonstrated a classical type of failure characterized by crushing of the concrete at compression zone. A normal crack pattern was observed which usually initiated within the flexural span between the test supports, as evidenced by Fig. 14. The cracks were mainly vertical and concentrated at the mid-span, indicating that the beam underwent pure bending. As the load was increased, additional flexural cracks were formed propagating away from the mid-span with more inclined as it approaches into the two test supports. As the load was increased, additional flexural cracks started within the shear span;

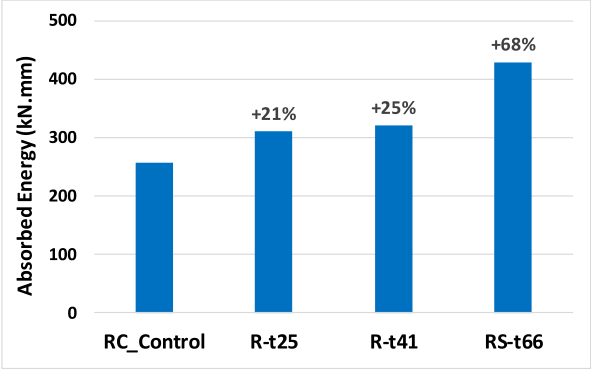

Fig. 12. Energy absorption capacity of repaired beams.

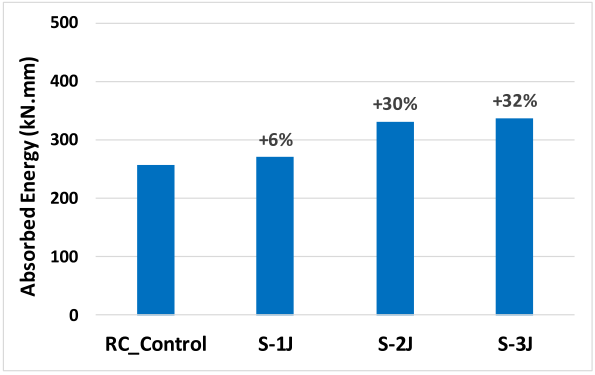

Fig. 13. Energy absorption capacity of strengthened beams.

however, because of the presence of shear stresses, the cracks became progressively more inclined and moved towards the two concentrated load points. Combined flexural-shear cracks were also observed especially at the middle thirds of the beam characterized by vertical-to-diagonal cracks, as can be seen in Fig. 14. At failure, most of the cracks ran through the whole beam surface with crack lengths ranging 35–161 mm. A total of eleven cracks appeared in the beam in which 2 cracks seen in the pure bending region in the mid-span that rapidly widened, and finally became the main cracks.

Likewise, the failure mode of all repaired RC beams (shown in Fig. 15) was predominantly governed by excessive yielding of the steel reinforcement up to crushing of top concrete. Based from visual observation of the specimen and the progressive load–deflection curve displayed on the monitor during the actual test, generally the failure of all repaired beams was by rupture of the FRGC overlaid layer within the mid-span, after yielding of the bottom steel reinforcement and before crushing of concrete in compression. A similar cracking pattern was observed for beam R-t25 which are constituted by flexural and shear cracks or their combinations depending on the location and widely distributed along its length as shown in Fig. 15a. Specifically, it was observed that the early crack development started at the beam soffit (i.e. tensile FRGC), followed by upward propagation perpendicular to the FRGC layers and extending to the concrete section until failure. It is worth-noting that the crack originating from the bottom of the repaired beam and later totally ruptured FRGC seamlessly extended the propagation up to the concrete component. When the load approached 31.3 kN (approximately 35% of the ultimate load), first flexural crack formed in the tensile zone of the concrete. As load increased, a large number of flexural cracks were developed on beam. Cracks were not concentrated at mid-section but spread all throughout the beam. This demonstrates the excellent bond performance of FRGC and that delamination is not a concern if this will be used in repairing concrete elements and that FRGC overlay or the concrete has the ability of diffusing totally the tensile stress without creating massive local stress concentration at the interface resulting to debonding failure. A thin horizontal crack was also noticeable in the interface between FRGC repair material and the concrete substrate but eventually no spalling of concrete cover was noticed. A similar cracking pattern was observed for beams R-t25 and R-t41 which are constituted by flexural and shear cracks or their combinations depending on the location and widely distributed along its length as shown in Fig. 15b and 15c. One distinction can be established between the two repaired beams and to its un-repaired counterpart which is that the cracks of the former is shorter and the number of cracks was lesser (9 and 8 visible cracks for both R-t25 and R-t41, respectively, as compared to 11 for control beam).

In the case of RS-t66, the cracking properties resembles that of the other repaired RC beams with horizontal hairline cracks occurred on the FRGC and concrete interface (shown Fig. 15d). RS-t66 demonstrated 7 visible fissures up to failure, value that is generally lower than both the

Table 7
Crack details and property.

Specimen ID	Crack length (mm)		Maximum crack Width (mm)	Cracks developed at the beam			Crack property
	Minimum	Maximum		Concrete substrate	FRGC	Total number of cracks	
RC_Control	35	161	2.45	11	0	11	Flexural-shear
R-t25	63	125	4.36	8	8	9	Flexural-shear
R-t41	77	139	7.34	8	8	8	Flexural-shear
RS-t66	42	150	5.74	4	6	7	Flexural-shear
S-1 J	48	151	7.91	9	8	10	Flexural-shear
S-2 J	116	129	3.54	–	4	4	Pure Flexure
S-3 J	36	159	5.56	–	5	5	Pure Flexure

Fig. 14. Condition of RC_Control at the end of the test.

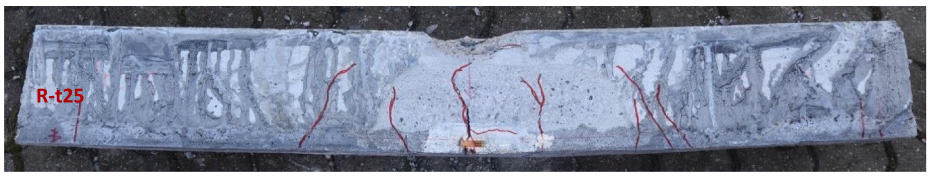

a. R-t25

b. R-t41

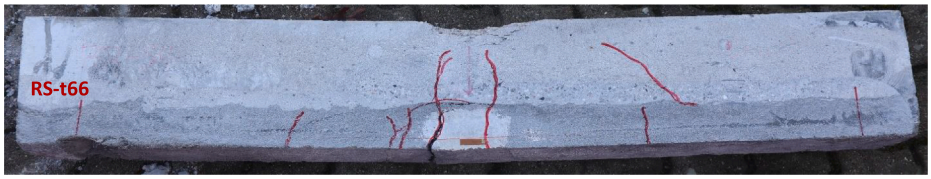

c. RS-t66

Fig. 15. Condition of repaired beams at the end of the test.

control and the other two repaired RC beams. For all repaired beams, it was observed that only one crack was totally opened at the final stage of the loading, just like what happened to the control beam. Regarding crack lengths of the repaired beams, Table 7 demonstrates that their corresponding values have ranged between 42 and 150 mm and intermediately falls within the values of the control specimen. The effectiveness of using FRGC to protect the deteriorated beams from possible re-deterioration can be seen from the decreased number of cracks in the concrete layer as shown in Table 7. It is apparent that a larger number of concrete cracks developed in the un-repaired beams (i.e. 10) as compared when an FRGC was overlaid with having only in the range of 4–8. Conclusively the application of FRGC overlays can enhance the cracking performance of the previously deficient RC beam.

Meanwhile, the cracking behavior of strengthened RC beams using bottom jacketing (S-1 J) looks similar with that of the repaired beams, with relatively few visible cracks than the un-repaired beams (shown in Fig. 18). As displayed in Table 7, number of cracks on RC layer is reduced by 20% by FRGC bottom jacket indicating its effectiveness to suppress the crack development of the RC layer during the entire testing process. The cracking direction was also observed to propagate seamlessly from the bottom FRGC to the upper concrete portion, as can be seen in Fig. 16a. Unlike the repaired beams, a horizontal cracking was detected within the layers of concrete instead in the FRGC-to-concrete interconnections. In the case of S-2 J, cracks are purely vertical and concentrated at the mid-section of the beam as shown on Fig. 16b. It can be observed that the number of cracks for S-2 J is less compared to the control specimen of having only 3 fissures. Post-mortem examination of the strengthened beam revealed that no delamination was observed between the FRGC and concrete substrate regardless of its interface location (i.e., compressive and tensile regions). In addition, spalling of

a. S-1J

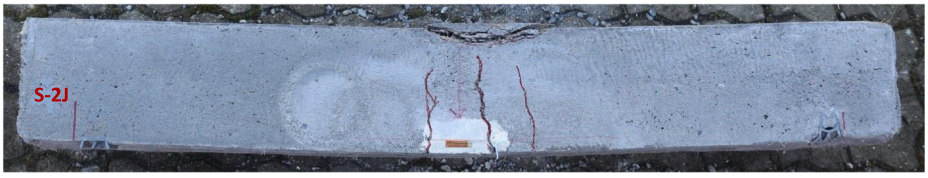

b. S-2J

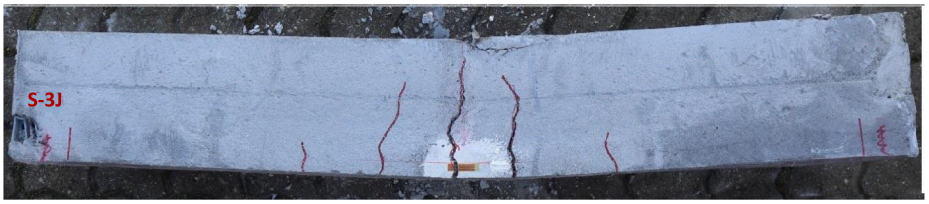

c. S-3J

Fig. 16. Condition of strengthened beams at the end of the test.

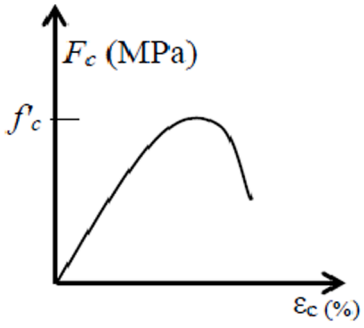

a. Concrete in compression

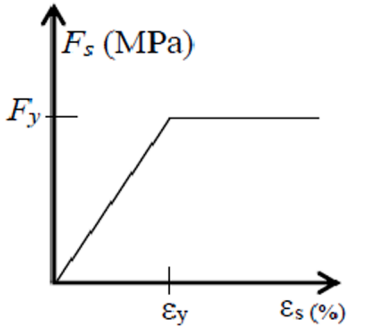

b. Steel rebar in tension

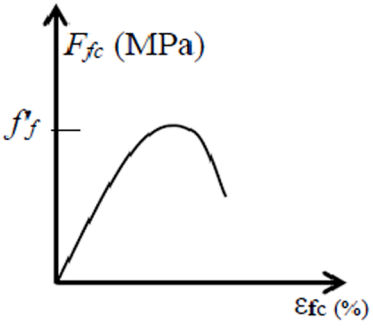

c. FRGC in compression

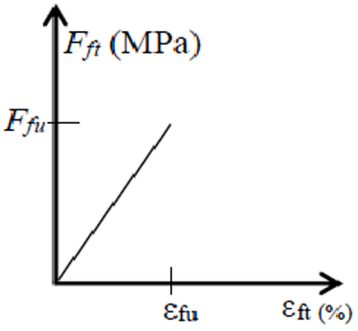

d. FRGC in tension

Fig. 17. Material model used in the analytical study.

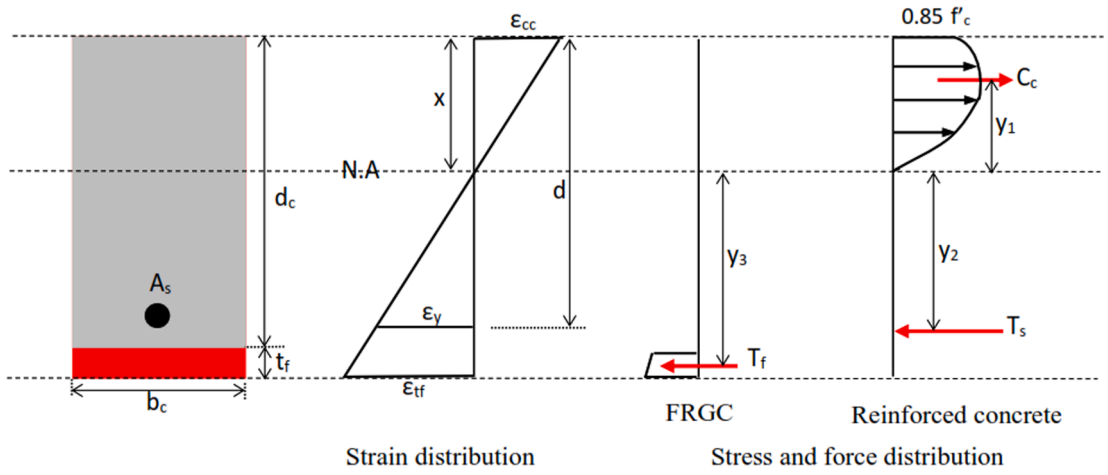

Fig. 18. Stress, strain and force distribution diagram for S-1 J.

FRGC on the two sides did not occur and were found to be intact with the concrete core even up to the failure loading conditions. This apparently indicates a good bonding property that FRGC and the proposed strengthening method could offer. In contrary to S-1 J and control beam, no diagonal shear cracks were noticeable indicating that using 2-side jacketing did not only improve the flexural performance of the beam but enhanced its shear capacity as well. S-2 J demonstrated crushing of FRGC and concrete at compression zone as the mode of failure. Cracks for S-3 J tend to become vertical indicating that the beam is predominantly subjected under pure bending as shown in Fig. 16c. It can also be perceived that beam jacketed on its three sides showed no shear crack even at the portion near the support region. Also, no spalling of FRGC on the bottom and sides was noticed and remained intact with the old RC beam. Beam S-3 J observed to have 5 visible cracks, a relatively smaller value compared to S-1 J and control beam. Like S-2 J, S-3 J exhibited multiple completely crack openings at the final loading stage and failed by crushing of FRGC and concrete under compression with no noticeable delamination at its different interface zones. In general, it is noted that the bonding between the FRGC strengthening layer and old concrete surface was sufficiently good, as no horizontal slip was noted in any of the beams regardless of the repair and strengthening configurations. Also it was observed that beams strengthened using these jacketing techniques in general did not show localized cracks in the additional FRGC layers. It may be concluded that using a needle scaler to roughen the surface of the concrete is already enough to ensure sufficient bonding with FRGC layers.

4. Prediction of flexural capacity of jacketed beams

The analytical model was developed to predict the flexural capacity in terms of ultimate moment of the tested beam and compared with the result obtained from the experiment. The simplified model is based on the combinations of the flexural formula described in ACI 318–19 [30], and the following assumptions: (1) the bond between all constituent materials including FRGC and concrete substrate is perfect, (2) the contributions of steel reinforcement in the compressive region and the concrete in tensile zone are neglected, (3) The stress–strain relationships of the concrete, steel reinforcement and FRGC follow the material behavior shown in Fig. 19. The first assumption particularly on the FRGC and concrete substrate bond maybe valid since no case of FRGC overlay delamination was observed during the conduct of experimental tests on repaired and strengthened RC beams after failure as discussed in Section 3.5. Fig. 17 indicates that concrete assumed a parabolic curve (Fig. 19a) while steel adheres to be perfectly elasto-plastic (Fig. 17b). In the case of FRGC, its compressive stress–strain behavior is somewhat similar to that of concrete as what had been observed in the experiment (load-deformation curve shown in Fig. 1), thus a parabolic relationship was considered (Fig. 17c). On the other hand, the curve of FRGC in tension adopts a softening behavior curve as shown in Fig. 17d since this behavior was observed during the uniaxial tensile test of FRGC. From the material model described in Fig. 17, the stress, strain and force distribution diagram of the strengthened beams was developed and displayed in Figs. 18–20. This diagram served as reference in the calculation of all internal forces and moments provided by the constituent materials. In the case of repaired beams (i.e., R-t25, R-t41 and RS- t66), the diagram

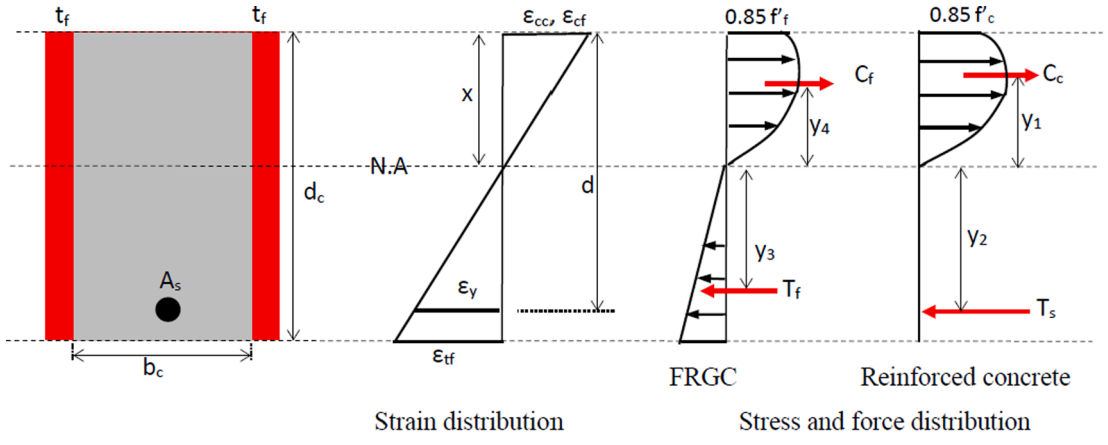

Fig. 19. Stress, strain and force distribution diagram for S-2 J.

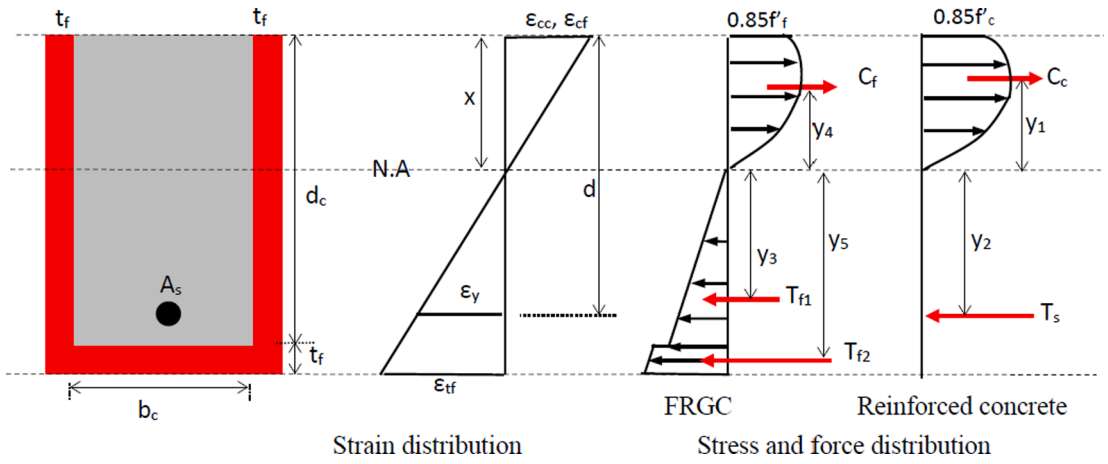

Fig. 20. Stress, strain and force distribution diagram for S-3 J.

and all calculations adopt that of the S-1 J. Figs. 18–20 demonstrates the superposition between the contributions of concrete in compression, steel reinforcement in tension and FRGC jacketing overlay in both compressive and tensile zones. At the ultimate condition, the steel reinforcement in the tensile zone yielded (F_y) while the concrete in the compressive region reaches its compressive strength, $f_c^{'}$. Also, FRGC simultaneously reaches its ultimate tensile strength, (for S-1 J and other repaired beams) or reaching of both tensile strength, F_{fu} and compressive strength, $f_f^{'}$ (for S-2 J and S-3 J), with stress distribution along the beam section following from the FRGC material model shown in Fig. 17.

The compressive and tensile forces of concrete, steel and FRGC are calculated in terms of the depth of the neutral axis from the top fiber section, x_c, and are summarized in Table 8. It is noted that compressive force for concrete and FRGC was calculated using an equivalent rectangular stress block suggested in ACI 318–19, and assumed that the factors relating to the depth of this equivalent block are similar for these two constituent materials (i.e., $\beta_1 = \beta_{1c} = \beta_{1f}$). The forces indicated in Tables 8-10 are used to calculate the value of the neutral axis depth, x_c, using the equilibrium of forces shown in Equation (1). In this study, the values of x_c was calculated using iterative process through a self-made program in an Excel spreadsheet.

$$\sum F(x) = \sum (T - C) = 0 \tag{1}$$

Equations (2)–(4) relates all forces in an equilibrium for specimens S-1 J, S-2 J and S-3 J, respectively.

$$A_s F_y + F_{fu} b_c t_f \left(\frac{d_c - x_c}{d_c - x_c + t_f}\right) + 0.5 F_{fu} b_c t_f \left(1 - \frac{d_c - x_c}{d_c - x_c + t_f}\right) - 0.85 f_c^{'} \beta_{1c} x_c b_c = 0 \tag{2}$$

$$A_s F_y + 0.5 F_{fu} 2 t_f (d_c - x_c) - 0.85 f_c^{'} \beta_{1c} x_c b_c - 0.85 f_f^{'} \beta_{1f} x_c 2 t_f = 0 \tag{3}$$

Table 8
Force and moment equations for S-1 J.

Force	$C_c = 0.85 f_c^{'} \beta_{1c} x_c b_c T_s = A_s F_y T_f = F_{fu} b_c t_f \left(\frac{d_c - x_c}{d_c - x_c + t_f}\right) + 0.5 F_{fu} b_c t_f \left(1 - \frac{d_c - x_c}{d_c - x_c + t_f}\right)$
Moment	$M = 0.85 f_c^{'} \beta_{1c} x_c b_c \left(x_c - x_c \frac{\beta_{1c}}{2}\right) + A_s F_y (d - x_c) + F_{fu} b_c t_f \left(\frac{d_c - x_c}{d_c - x_c + t_f}\right) \left(d_c - x_c + \frac{t_f}{2}\right) + 0.5 F_{fu} b_c t_f \left(1 - \frac{d_c - x_c}{d_c - x_c + t_f}\right) \left(d_c - x_c + \frac{2t_f}{3}\right)$

Table 9
Force and moment equations for S-2 J.

Force	$C_c = 0.85 f_c^{'} \beta_{1c} x_c b_c C_f = 0.85 f_f^{'} \beta_{1f} x_c 2 t_f T_s = A_s F_y T_f = 0.5 F_{fu} 2 t_f (d_c - x_c)$
Moment	$M = 0.85 f_c^{'} \beta_{1c} x_c b_c \left(x_c - x_c \frac{\beta_{1c}}{2}\right) + 0.85 f_f^{'} \beta_{1f} x_c 2 t_f \left(x_c - x_c \frac{\beta_{1f}}{2}\right) + A_s F_y (d - x_c) + 0.5 F_{fu} 2 t_f (d_c - x_c) \left(\frac{2(d_c - x_c)}{3}\right)$

Table 10
Force and moment equations for S-3 J.

Force	$C_c = 0.85 f_c^{'} \beta_{1c} x_c b_c C_f = 0.85 f_f^{'} \beta_{1f} x_c 2 t_f T_s = A_s F_y T_{f1} = 0.5 F_{fu} 2 t_f (d_c - x_c) \left(1 - \frac{d_c - x_c}{d_c - x_c + t_f}\right) T_{f2} = F_{fu} b_c t_f \left(\frac{d_c - x_c}{d_c - x_c + t_f}\right) + 0.5 F_{fu} b_c t_f \left(1 - \frac{d_c - x_c}{d_c - x_c + t_f}\right)$
Moment	$M = 0.85 f_c^{'} \beta_{1c} x_c b_c \left(x_c - x_c \frac{\beta_{1c}}{2}\right) + 0.85 f_f^{'} \beta_{1f} x_c 2 t_f \left(x_c - x_c \frac{\beta_{1f}}{2}\right) + A_s F_y (d - x_c) + F_{fu} b_c t_f \left(\frac{d_c - x_c}{d_c - x_c + t_f}\right) \left(d_c - x_c + \frac{t_f}{2}\right) + 0.5 F_{fu} b_c t_f \left(1 - \frac{d_c - x_c}{d_c - x_c + t_f}\right) \left(d_c - x_c + \frac{2t_f}{3}\right)$

$$A_s F_y + 0.5 F_{fu} 2 t_f (d_c - x_c) \left(1 - \frac{d_c - x_c}{d_c - x_c + t_f}\right) + F_{fu} b_c t_f \left(\frac{d_c - x_c}{d_c - x_c + t_f}\right) + 0.5 F_{fu} b_c t_f \left(1 - \frac{d_c - x_c}{d_c - x_c + t_f}\right) - 0.85 f_c^{'} \beta_{1c} x_c b_c - 0.85 f_f^{'} \beta_{1f} x_c 2 t_f = 0 \tag{4}$$

where A_s is total area of bottom reinforcement bars; F_y and F_{fu} is the yield and ultimate tensile strength of rebar and FRGC, respectively; $f_c^{'}$ and $f_f^{'}$ is the compressive strength of concrete and FRGC at 28 days, β_{1c} and β_{1f} are factors relating to the depth of the equivalent stress block defined in ACI 318–19; d, d_c, b_c, t_f are geometric dimensions of the jacketed beams illustrated in Figs. 18–20.

After determining x_c, the theoretical ultimate moment capacity can now be computed by summing all forces and its corresponding moment arm from the neutral axis, as shown in Table 1.

The comparison between the predicted values and that obtained from experiment was done in terms of its ultimate (peak) moment capacity, denoted as M_{uT} and M_{uE}, respectively. To do this, M_{uE} were obtained from the experimental ultimate (peak) load, P_{uE} , summarized in Table 5 using equation (5).

$$M_{uE} = P_{uE} \left(\frac{L_n - x_n}{4}\right) \tag{5}$$

where L_n is the effective testing span and x_n is the distance between

the two-point loads in the flexural testing set-up as shown in Fig. 5. Considering the geometrical and mechanical properties of the concrete, steel reinforcement and FRGC, as well as factor coefficients provided in ACI 318–19, the ultimate moments, M_{uT} and M_{uE} were finally calculated using self-made program in an Excel spreadsheet. The comparison between the values obtained from analytical and experimental studies is summarized in Table 11. The result indicated in the table that using this model yielded an error of prediction in the range of 4–7%. In general, the calculated results of the ultimate moment capacity of the repaired and strengthened RC beams agree reasonably with the experimental data.

5. Conclusions

The present work investigated the flexural behavior of RC beams repaired and strengthened by hybrid FRGC using different jacketing configurations. Twelve FRGC-jacketed and two control RC beams were subjected to four-point bending test to determine their loading performance, cracking response, ductility and energy absorption capacity. The following are the conclusions based from the experimental and analytical results.

- The FRGC-repaired beams exhibited an increase in cracking, yielding and ultimate load of 28–58%, 8–35%, and 10–33%, respectively, compared to control beam, indicating that this repairing method is successful in at least restoring the loading performance of the initial RC beam. RC beams repaired by 25–41 mm thick FRGC showed 3–8% and 21–25% higher ductility and toughness, respectively, than the control beam. Although the addition of monolithic 66 mm thick FRGC resulted to 4% reduced ductility, it was able to enhance the energy absorption value of the initial RC beam by 68%.
- Strengthening using 25 mm thick FRGC jackets on the bottom, 2 and 3 sides of the RC beam resulted to its 94–167% and 24–62% load enhancement at the first cracking and yielding conditions, respectively. On the other hand, it also increased the ultimate load value of the initial RC beam by 21–62%. RC beams strengthened along the 2 sides shown matchable ductility and 30% higher absorption capacity than the control specimen. In contrary, RC beams strengthened on the bottom and 3 sides demonstrated less ductile response, nevertheless their energy absorption value capacity is higher than their unstrengthened counterpart by 6–32%.
- FRGC jacketing system is more significant in improving the first cracking performance of the initial RC beam rather than the yield and ultimate responses regardless of the repair and strengthening configurations.
- Jacketed RC beams showed no sign of overlay delamination up to failure irrespective of the repair and strengthening patterns, confirming an excellent bond between the FRGC and concrete substrate. All FRGC repaired beams and beam strengthened on the bottom side have flexural and shear cracks indicating similar cracking behavior with the ordinary RC beam. However, the former demonstrated lesser number of cracks than the latter pointing out the effectiveness of FRGC overlay as protective layer for crack control in the composite beams. Strengthening using FRGC jackets on the 2 and 3 sides only manifest flexural cracks, indicating that not only that it enhances the flexural capacity but also improved the shear performance of the RC beam.
- The model predicting the flexural moment capacity of the FRGC jacketed beams compared reasonably with the experimental results with 4–7% margin of difference.

In general, the proposed strengthening technique exhibited positive effect in enhancing the flexural performance of RC beams. However, further investigation is needed in comparing the proposed method to commercially-produced engineered cementitious composite (ECC) materials used in repair/strengthening for its wide acceptance.

Table 11
Predicted and experimental ultimate moment capacity of FRGC-jacketed beams.

Specimen ID	M_{uT} (kN–m)	M_{uE} (kN–m)	Difference (%)
R-t25	7.81	8.16	4.3
R-t41	8.10	8.67	6.6
RS-t66	9.26	9.85	6.0
S-1 J	8.36	8.99	7.1
S-2 J	9.37	10.07	7.0
S-3 J	11.35	11.99	5.4

CRediT authorship contribution statement

Ernesto J. Guades: Conceptualization, Methodology, Project administration, Writing - original draft, Writing - review & editing. **Henrik Stang:** Methodology, Project administration, Writing - original draft, Writing - review & editing. **Jacob W. Schmidt:** Methodology, Writing - original draft, Writing - review & editing. **Gregor Fischer:** Methodology, Writing - original draft, Writing - review & editing.

Declaration of Competing Interest

The authors declare that they have no known competing financial interests or personal relationships that could have appeared to influence the work reported in this paper.

Acknowledgement

This project has received funding from the European Union's Horizon 2020 Research and Innovation Programme under the Marie Sklodowska-Curie grant agreement No. 713683.

Appendix A. Supplementary data

Supplementary data to this article can be found online at https://doi.org/10.1016/j.engstruct.2021.112053.

References

[1] Ding Y, Bai YL. Fracture properties and softening curves of steel fibre-reinforced slag-based geopolymer mortar and concrete. Mater. 2018;11:1–18.
[2] Alanazi H, Yang M, Zhang D, Gao Z. Bond strength of PCC pavement repairs using metakaolin-based geopolymer mortar. Cem Concr Compos 2016;65:75–82.
[3] Hu S, Wang H, Zhang G, Ding Q. Bonding and abrasion resistance of geopolymeric repair material made with steel slag. Cem Concr Compos 2008;30(3):239–44.
[4] Hussein M, Kunieda M, Nakamura H. Strength and ductility of RC beams strengthened with steel-reinforced strain hardening cementitious composites. Cem Concr Compos 2012;34:1061–6.
[5] Zanotti C, Borges PHR, Bhutta A, et al. Bond strength between concrete substrate and metakaolin geopolymer repair mortar: effect of curing regime and PVA fibre reinforced. Cem. Concr. Compos. 2017;80:307–16.
[6] Kong DLY, Sanjayan JG. Damage behavior of geopolymer composites exposed to elevated temperatures. Cem Concr Compos 2008;30:986–91.
[7] Olivia M, Nikraz H. Properties of fly ash geopolymer concrete designed by Taguchi method. Mater. Des. 2012;36:191–8.
[8] Y. Cui, O. Kayali, T. Zhao, C. Zhang, Bond strength of steel bar and plain or fibre-reinforced geopolymer concrete, World Congress on Advances in Structural Engineering and Mechanics, 2017, Seoul, Korea, 1–14.
[9] Matthews J, Selvakumar A, Vaidya S. Large-diameter sewer rehabilitation using a spray-applied fibre-reinforced geopolymer mortar. ASCE Pract. Period. Struct. Des. Constr. 2015;20(4):1–6.
[10] https://infrastructure.milliken.com. Date accessed: 2 May 2019.
[11] Müller S, Mechtcherine V. Use of strain-hardening cement-based composites (SHCC) for retrofitting. ICCRRR MATEC Web. Conf. 2018;199:1–6.
[12] Al-Majidi MH, Lampropoulos A, Cundy AB, et al. A novel corrosion resistance repair technique for existing reinforced concrete [RC] elements using polyvinyl alcohol fibre reinforced geopolymer concrete (PVAFRGC]. Constr Build Mater 2018;164:603–19.
[13] Sial SU, Khan MI. Performance of strain hardening cementitious composite as strengthening and protective overlay in flexural members. ICCRRR MATEC Web. Conf. 2018;199:1–8.
[14] Arezoumandi M, Wirkman C, Volz JS. Performance of fibre-reinforced self-consolidating concrete for repair of bridge substructures. Structures 2018;15:320–8.

[15] Zaher YA, Abdel Aziz YH. Effect of elevated temperature on RC pre-cracked beams repaired and strengthened using jackets of cementitious materials. I J Civil Engg Technol 2017;8(5):819–31.
[16] Sukontasukkul P, Pongsopha P, Chindaprasirt P, et al. Flexural performance and toughness of hybrid steel and polypropylene fibre reinforced geopolymer. Constr. Build. Mater. 2018;161:37–44.
[17] Mastali M, Dalvand A, Sattarifardc AR, et al. Characterization and optimization of hardened properties of self-consolidating concrete incorporating recycled steel, industrial steel, polypropylene and hybrid fibres. Compos. Part B-Eng. 2018;151:186–200.
[18] Shaikh FUA, Maalej M, Paramasivam P. Flexural responses of hybrid steel–polyethylene fibre reinforced cement composites containing high volume fly ash. Constr. Build. Mater. 2007;21:1088–97.
[19] A. Bentur, S. Mindess, Fibre reinforced cementitious composites, Modern Concrete Technology Series: Taylor & Francis (2009).
[20] Shaikh FUA. Review of mechanical properties of short fibre reinforced geopolymer composites. Constr. Build. Mater. 2013;43:37–49.
[21] Hasholt MT, Christensen KU, Pade C. Frost resistance of concrete with high contents of fly ash - A study on how hollow fly ash particles distort the air void analysis. Cem Concr Res 2019;119:102–12.
[22] Plizzzari GA. Fibre Reinforced Concrete for repairing and strengthening RC structures: some recent advancements. ICCRRR MATEC Web. Conf. 2018;199:1–11.
[23] Diab YG. Strengthening of RC beams by sprayed concrete: experimental approach. Engg Struc 1998;20(7):631–43.
[24] Pam HJ, Kwan AKH, Islam MS. Flexural strength and ductility of reinforced normal- and high-strength concrete beams. Struct Build 2000;146(4):381–9.
[25] Meda A, Minelli F, Plizzari GA. Flexural behaviour of RC beams in fibre-reinforced concrete. Compos B 2012;43:2930–7.
[26] Al-Osta MA, Isa MN, Baluch MH, Rahman MK. Flexural behavior of reinforced concrete beams strengthened with ultra-high performance fibre reinforced concrete. Constr Build Mater 2017;134:279–96.
[27] Nematollahi B, Sanjayan J, Shaikh FUA. Comparative deflection hardening behavior of short fibre reinforced geopolymer composites. Constr. Build. Mater. 2014;70:54–64.
[28] Ostertag CP, Blunt J. Hybrid fibre reinforced concrete for use in bridge approach slabs. Proc. CBM-CI Intl. Workshop 2008:73–90.
[29] Banthia N, Nandakumar N. Crack growth resistance of hybrid fibre reinforced cement composites. Cem. Concr. Compos. 2003;25:3–9.
[30] ACI. 318–19, Building Code Requirements for Structural Concrete and Commentary. American Concrete Institute 2019.